Decomposing the linear momentum transfer components in break-up fusion reactions: An experimental study of the $^{19}F + ^{159}Tb$ system

M. Shariq Asnain,[1,*] Mohd. Shuaib,[1] Ishfaq Majeed,[1] Manoj Kumar Sharma,[2] Abhishek Yadav,[3] Devendra P. Singh,[4] Pushpendra P. Singh,[5] R. Kumar,[6] B. P. Singh,[1,†] and R. Prasad[1]

[1]*Department of Physics, Aligarh Muslim University, Aligarh-202 002, Uttar Pradesh, India*
[2]*Department of Physics, University of Lucknow, Lucknow-226007, Uttar Pradesh, India*
[3]*Department of Physics, Faculty of Natural Sciences, Jamia Millia Islamia, New Delhi-110025, India*
[4]*Department of Physics, University of Petroleum and Energy Studies, Dehradun-248 007, Uttarakhand, India*
[5]*Department of Physics, Indian Institute of Technology, Ropar-140 001, Punjab, India*
[6]*Inter University Accelerator Centre, Aruna Asaf Ali Marg, New Delhi-110067, India*

(Received 9 June 2022; revised 27 October 2022; accepted 30 November 2022; published 20 December 2022)

In the present work, measurement and analysis of forward recoil range distribution of various reaction residues populated in the interaction of ^{19}F projectile with ^{159}Tb target nucleus have been performed. The aim is to disentangle the contribution of complete fusion (CF) and incomplete fusion (ICF) components at two different above-barrier energies ≈83 and 94 MeV. The recoil-catcher technique with off-line γ-ray spectroscopy has been performed. The complete and incomplete fusion events have been identified by full and partial linear momentum transfer, respectively. A single Gaussian distribution has been observed in case of residues populated via complete fusion processes. However, the recoil range distribution for α-emitting channels was found to be deconvoluted into more than one Gaussian peak indicating the involvement of both full and partial linear momentum transfer components due to the presence of CF and ICF processes. The analysis of data suggests that projectile breaks up as soon as it comes near the vicinity of target nuclear field leading to different linear momentum transfer components. Further, the analysis done within the framework of universal fusion function indicates a significant break-up fusion probability of ^{19}F projectile. As such, at lower energies ^{19}F is found to behave similar to other α-cluster beams.

DOI: 10.1103/PhysRevC.106.064607

I. INTRODUCTION

The study of projectile break up in heavy-ion (HI) reactions has been a topic of interest in nuclear physics in recent years. At relatively low projectile energies (≈ 4–7 MeV/nucleon), it is established that the most dominant modes of reactions are complete fusion (CF) and incomplete fusion (ICF) processes. The recent measurements show that these processes start competing at energies just above the Coulomb barrier [1–5]. In case of CF, all nucleonic degrees of freedom are involved due to fusion of entire projectile mass carrying input angular momenta $\ell < \ell_{crit}$. Such fusion leads to the formation of an equilibrated compound nucleus (CN). However, in case of ICF reactions, the fusion of the entire projectile with the target nucleus is hindered for the partial waves carrying angular momenta $\ell > \ell_{crit}$. At these higher values of ℓ, the repulsive centrifugal potential starts increasing resulting in the fact that the attractive nuclear potential may not sustain the fusion of the entire projectile. In order to provide the sustainable angular momentum required for fusion, the projectile may break up into fragments(s) and one of the fragment(s) fuses with the target nucleus, whereas the remnant continues to move in the forward direction without any interaction. The γ-multiplicity experiments performed by Inamura *et al.* [6] and Wilczynski *et al.* [7] showed that occurrence of ICF involves $\ell > \ell_{crit}$. On the other hand, Tserruya *et al.* [8], from the measurements carried out on spherical targets, indicated the observation of ICF even for $\ell < \ell_{crit}$. A pictorial representation CF and ICF processes is shown in Fig. 1. In order to have a better insight on ICF processes, theoretical models viz., the break-up fusion (BUF) model [9,10], the sum-rule model [11,12], the exciton model [13,14], etc. have also been proposed. It has been observed that the above-mentioned models satisfactorily explain ICF data at energies ⩾10 MeV/nucleon but are unable to explain such processes satisfactorily at lower energies (≈4–7 MeV/nucleon), which is the energy regime of the present work. However, the onset of ICF at energies just above the Coulomb barrier has invigorated to investigate ICF reaction dynamics at low energies [5]. Moreover, recent investigations on heavy-ion interactions have also indicated the presence of preequilibrium (PEQ) reactions at low energies [15]. In case of PEQ reactions, emission of particles may take place even before the establishment of statistical equilibrium of the composite system. It may happen that a few nucleons may get ejected even before the statistical equilibrium of the compound nucleus is achieved. The emission of such

*asnainshariq@gmail.com
†bpsinghamu@gmail.com

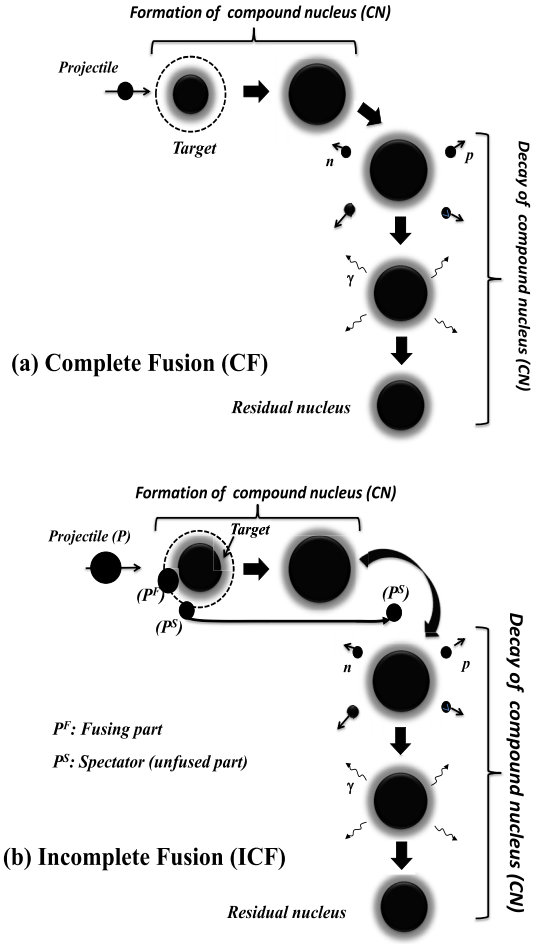

FIG. 1. The pictorial representation of (a) Complete fusion (CF) and (b) incomplete fusion (ICF) processes.

particles is referred to as preequilibrium emission. The time scale involved in case of PEQ reactions is typically $\approx 10^{-18}$–10^{-20} s or so, whereas the time scale for evaporation after establishment of equilibrium (or CN processes) is $\approx 10^{-16}$ s. On the other hand, in case of direct reactions, the projectile interacts with a single or only a few nucleons of the target nucleus. The time taken by the projectile to traverse the target nucleus is very short ($\approx 10^{-22}$ s). The investigation of PEQ reactions has been performed from the analysis of excitation function (EF), forward recoil range distribution (FRRD), and spin distribution (SD) measurements in case of heavy-ion reactions [15].

The break up or partial fusion of projectile leads to fractional linear momentum transfer from projectile to the target nucleus. Consequently, the composite nucleus formed in case of ICF is likely to have shorter range in the stopping medium as compared to that formed in case of CF reactions. As such, the measurement of forward recoil range distributions (FRRDs) may be used as one of the most direct and irrefutable methods to distinguish the various CF and ICF components. In FRRD measurements, the residues populated via CF and ICF processes will correspond to different characteristic velocity distribution. Therefore, the distribution of experimentally measured yields of different reaction residues as a function of velocity and/or range in stopping medium, may give a better insight into the reaction mechanism involved in such reactions. Further, the FRRD measurements has been capable of deciphering the relative contributions of compound and precompound components and hence may be used a promising method to study the reaction dynamics involved in case of heavy-ion (HI) reactions.

With this motivation, an attempt has been made to have a detailed investigation on ICF reaction dynamics from the analysis of forward recoil range distribution (FRRD) of heavy residues populated via CF and/or ICF routes. In the present work, the FRRDs of different reaction residues populated in the interaction of ^{19}F with ^{159}Tb, have been measured at two distinct beam energies 82.8 and 94.3 MeV. This paper is organized as follows: A brief description of experimental details is given in Sec. II. The Sec. III deals with the measurement and analysis of FRRDs and finally the conclusion is given in Sec. IV.

II. EXPERIMENTAL DETAILS

The experiments for the measurement of FRRDs for $^{19}\mathrm{F} + {}^{159}\mathrm{Tb}$ system have been performed at the Inter University Accelerator Center (IUAC), New Delhi, India. The $^{19}\mathrm{F}^{8+}$ ion beam was delivered using the 15UD Pelletron accelerator facility. Two different stacks, each consisting of ^{159}Tb target (abundance = 100%) followed by a series of thin Al-catcher foils were irradiated separately at ≈83 and 94 MeV beam energy. The ^{159}Tb target (thickness $\approx 350\,\mu\mathrm{g/cm^2}$) was deposited by the vacuum evaporation technique on Al foil (thickness $\approx 2.03\,\mathrm{mg/cm^2}$). The ^{159}Tb was mounted in such a way that the ^{19}F beam first faces Al foil so that after the energy loss in Al foil, the beam of required energy may fall on the target. A series of thin Al-catcher foils (sufficient enough to stop the CN formed via full momentum transfer) in the form of stack was placed just after the target so that the recoiling residues populated via CF and/or ICF processes could be trapped at their respective ranges in thin Al-catcher foils. A typical arrangement of experimental setup is shown in Fig. 2. In order to have better resolution in recoil ranges of the residues, the thickness of Al catchers were kept ≈ 15–$100\,\mu\mathrm{g/cm^2}$. The thicknesses of each catcher foil used for trapping the recoiling residues at 94.3 MeV and 82.8 MeV beam energy is given in Table I. From the kinematics, it was estimated that the heavy recoiling residues are mainly focused within a forward narrow cone of maximum 10°. As a representative case, the angular distribution of ^{174}W and ^{173}W residues populated via $4n$ and $5n$, respectively, at ≈83 MeV obtained from PACE [16] calculations indicate that most of the residues are emitted in the forward cone of angle up to 7°, which clearly indicates that the emission of residues is forward peaked. The size of the catcher foils of 10 mm diameter was more than sufficient to trap the recoiling heavy residues. The thickness of the target and each Al-catcher foils was measured by α-transmission method, which is based on the energy lost by 5.486 MeV α particles of standard ^{241}Am source while passing through the foil. The thickness of target and each Al-catcher foils was

TABLE I. Thickness of aluminium catcher foil used to trap the recoiling residues at 94.3 and 82.8 MeV beam energy.

$E_{lab} = 94.3$ MeV			$E_{lab} = 82.8$ MeV		
Catcher Foil No.	Thickness (μg/cm^2)	Cumulative Thickness (μg/cm^2)	Catcher Foil No.	Thickness (μg/cm^2)	Cumulative Thickness (μg/cm^2)
B1	59.5	59.5	D1	69.5	69.5
B2	44.2	103.7	D2	51.9	121.4
B3	53.2	156.9	D3	46.8	168.2
B4	17.8	174.7	D4	26.9	195.1
B5	25.7	200.4	D5	27.5	222.6
B6	45.8	246.2	D6	18	240.67
B7	33.7	279.9	D7	25.7	266.3
B8	34.3	314.2	D8	29.2	295.5
B9	35.5	349.7	D9	49.6	345.1
B10	40.7	390.4	D10	48.3	393.4
B11	44.2	434.6	D11	34.5	427.9
B12	42.5	477.1	D12	35.5	463.4
B13	45.8	522.9	D13	36.6	500
B14	45	567.9	D14	40.9	540.9
B15	40.8	608.7	D15	50.5	591.4
B16	41.8	650.58	D16	36.6	628
B17	45	695.5	D17	39.2	667.2
B18	50.2	745.7	D18	43	710.2
B19	52.5	798.2	D19	44.4	754.6
B20	63	861.2	D20	50.8	805.4
B21	98	959.2	D21	55.5	860.9

determined at several places by slightly shifting its position with respect to α source. Due to nonuniformity in sample thickness the measured thicknesses were found to have an uncertainty <2%. Further, the target and catcher foils were pasted on rectangular aluminium holders of size 2.5 × 2.0 cm^2 having concentric hole of diameter 1.0 cm, defining their geometric size. Each irradiation was carried out for ≈12 h in the general purpose scattering chamber (GPSC) [17]. The delay time between stopping of beam irradiation and starting of counting was minimized by taking out the irradiated foils using the in-vacuum transfer (ITF) facility. The beam flux

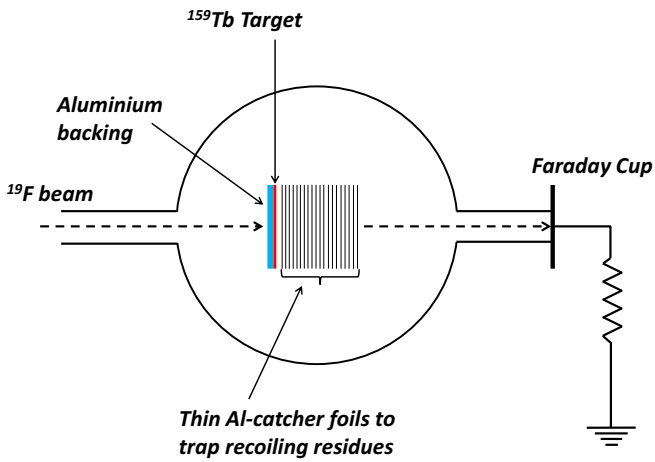

FIG. 2. A typical arrangement of target-catcher assembly used for FRRD measurements in the GPSC.

was calculated with the help of total charge collected in the Faraday cup placed just behind the stack. Proper care was taken to maintain the beam current to be constant. Further, during the irradiation, the fluctuations in the beam current were monitored and necessary corrections were made in the calculations. After the irradiation, the sample-catcher assembly was taken out of the scattering chamber and the activity induced in each catcher foil was recorded separately using a precalibrated high-resolution HPGe γ spectrometer (100 cc active volume) coupled to CAMAC-based CANDLE [18] software. The HPGe detector (resolution ≈2 keV for 1.33 MeV γ ray of ^{60}Co) was calibrated both for energy and efficiency. The efficiency of the HPGe detector at various source-detector distances was determined using standard ^{152}Eu γ source of known strength. Also, corrections for the dead time were also employed during the analysis. The γ-ray spectrum for the present system ^{19}F + ^{159}Tb showing the population of γ activities for different reaction residues formed via CF and/or ICF processes at a depth of ≈345 μg/cm^2 at 82.8 MeV beam energy is shown in Fig. 3. The different residues populated in the interaction of ^{19}F + ^{159}Tb system were identified on the basis of their characteristic γ-ray energies and further confirmed by the decay curve analysis. After the identification and confirmation of the residues, the production cross sections of the reaction products have been determined. Further, the measured γ-ray spectra did not show any evidence of signature of breakup α-induced fusion. It may also be remarked that two very close characteristic γ lines of 292.5 keV and 292.2 keV, respectively, due to ^{170}Lu(αp3n) and ^{171}Hf(α3n) residues are given in literature. Similarly, the residues ^{171}Hf(α3n)

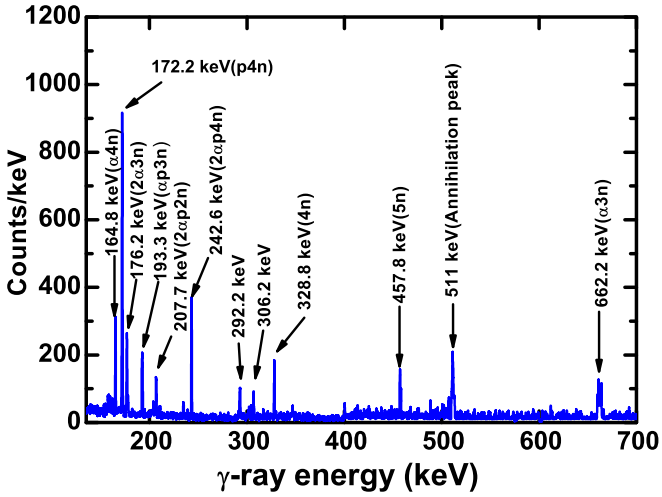

FIG. 3. The measured γ-ray spectrum due to residues populated via CF and/or ICF processes in $^{19}\mathrm{F} + ^{159}\mathrm{Tb}$ system recorded at 82.8 MeV beam energy for catcher foil number D9 placed at a cumulative depth of $\approx$345 μg/cm^2. The spectrum was recorded after 25 min of the stopping of irradiation.

and ^{173}Ta(p4n) have characteristics γ line of 305.6 keV and 306.2 keV, respectively. Since these γ lines are very close and due to limited resolution ($\approx$2 keV) of the spectrometer set up, these could not be resolved. Further, cross section for their population has not been calculated using these lines, and hence not assigned to a particular residue.

III. ANALYSIS AND EXPERIMENTAL RESULTS

A. Measurement of production yield and estimation of FRRD

In the present work, the analysis of FRRDs for different evaporation residues (ERs) populated via CF and/or ICF processes has been performed. As already mentioned earlier, the measurement of projected ranges of reaction products gives the degree of linear momentum transfer (ρ_{LMT}) from projectile to the target nucleus. The velocity distribution of a given type of reaction product is symmetric about the mean velocity (v_o) whose width may depend upon the mode of reaction. The mean velocity v_o may be given as

$$v_o = v_{\mathrm{CN}} = \frac{\sqrt{2M_P E}}{M_{\mathrm{CN}}}, \tag{1}$$

where M_P is the mass of projectile, $M_{\mathrm{CN}}(= M_P + M_T)$ is the mass of composite system (projectile+target), and E is the energy of projectile nucleus. Assuming the target at rest in HI collision process, the incident heavy ion has the linear momentum P_{proj}, which is imparted to the target. Considering the head-on collision, the degree of linear momentum transfer (P_{LMT}) will depend on the fraction of projectile getting fused with the target nucleus. As such,

$$\rho_{\mathrm{LMT}} = \frac{P_{\mathrm{frac}}}{P_{\mathrm{proj}}}, \tag{2}$$

where, P_{frac} is the linear momentum of the fused part of the projectile and P_{proj} is the linear momentum of the entire projectile. The ρ_{LMT} is proportional to the fused mass of the projectile and hence maximum linear momentum transfer (LMT) may give rise to maximum recoil velocity to the CN and hence maximum range in stopping medium. It is a promising way for determining the amount of LMT involved in a reaction process.

TABLE II. List of identified reaction residues in $^{19}\mathrm{F} + ^{159}\mathrm{Tb}$ system with their spectroscopic properties.

Residue	Half-life	J^π	E_γ (keV)	I$_\gamma$ (%)
^{174}W(4n)	29 min	0^+	328.8	9.25
^{173}W(5n)	7.6 min	$5/2^-$	457.8	44
^{173}Ta(p4n)	3.14 hr	$5/2^-$	172.2	17.4
^{171}Hf($\alpha 3n$)	12.1 hr	$7/2^+$	662.2	9.27
^{170}Hf($\alpha 4n$)	16.01 hr	0^+	164.8	87
^{170}Lu(αp3n)	2.01 d	0^+	193.3	2.07
^{167}Yb($2\alpha 3n$)	17.5 min	$5/2^-$	176.2	20.4
^{167}Tm(2αp2n)	9.2 d	$1/2^+$	207.7	43
^{165}Tm(2αp4n)	7.7 hr	$1/2^+$	242.6	35

The production cross section (σ_{ER}) of various identified reaction residues was computed using the standard formulation [19]. In order to obtain the normalized yields, the cross section of residues in each Al-catcher foil was divided by its thickness. The resulting normalized yields were plotted as a function of cumulative catcher depth in order to obtain the range distribution of identified reaction residues viz., ^{174}W($4n$), ^{173}W($5n$), ^{173}Ta($p4n$), ^{171}Hf($\alpha 3n$), ^{170}Hf($\alpha 4n$), ^{170}Lu($\alpha p3n$), ^{167}Yb($2\alpha 3n$), ^{167}Tm($2\alpha p2n$), and ^{165}Tm($2\alpha p4n$). The spectroscopic properties of the identified residues are given in Table II. As a representative case, the measured FRRDs for the reaction residues ^{173}W($5n$), ^{171}Hf($\alpha 3n$), ^{170}Lu($\alpha p3n$), ^{167}Yb($2\alpha 3n$), and ^{165}Tm($2\alpha p4n$) are shown in Figs. 4(a)–4(j) at both the studied energies, 82.8 and 94.3 MeV. A comparison of FRRD for residues ^{173}W populated via $5n$ channel at 82.8 MeV and 94.3 MeV is shown in Figs. 4(a) and 4(d), respectively. As can be seen from these figures, the measured FRRDs for this reaction shows only a single Gaussian peak indicating the involvement of only one linear momentum transfer (LMT) component in the production of this residue. Therefore, the ^{173}W residues are populated via full linear momentum transfer due to complete fusion process only. From close observation of the recoil range distribution of ^{173}W residues from Figs. 4(a) and 4(d), it is clear that the peak shifts towards a higher cumulative thickness as the beam energy is increased, as expected. It may be pointed out that the particle emission from the forward recoiling residues may change the energy and momentum of the final residue depending on the direction of emission. This is reflected in the width (FWHM) of the experimentally measured recoil range distributions. Further, any spread in the distribution may also be due to range straggling and influences from particle evaporation in the trajectory of the compound nucleus. Further, in case of α-emitting channels, the residues ^{171}Hf, ^{170}Hf, ^{170}Lu, ^{167}Yb, ^{167}Tm, and ^{165}Tm are expected to be populated via $\alpha 3n$, $\alpha 4n$, $\alpha p3n$, $2\alpha 3n$, $2\alpha p2n$, and $2\alpha p4n$ channels, respectively. The observed FRRDs for αxn channels

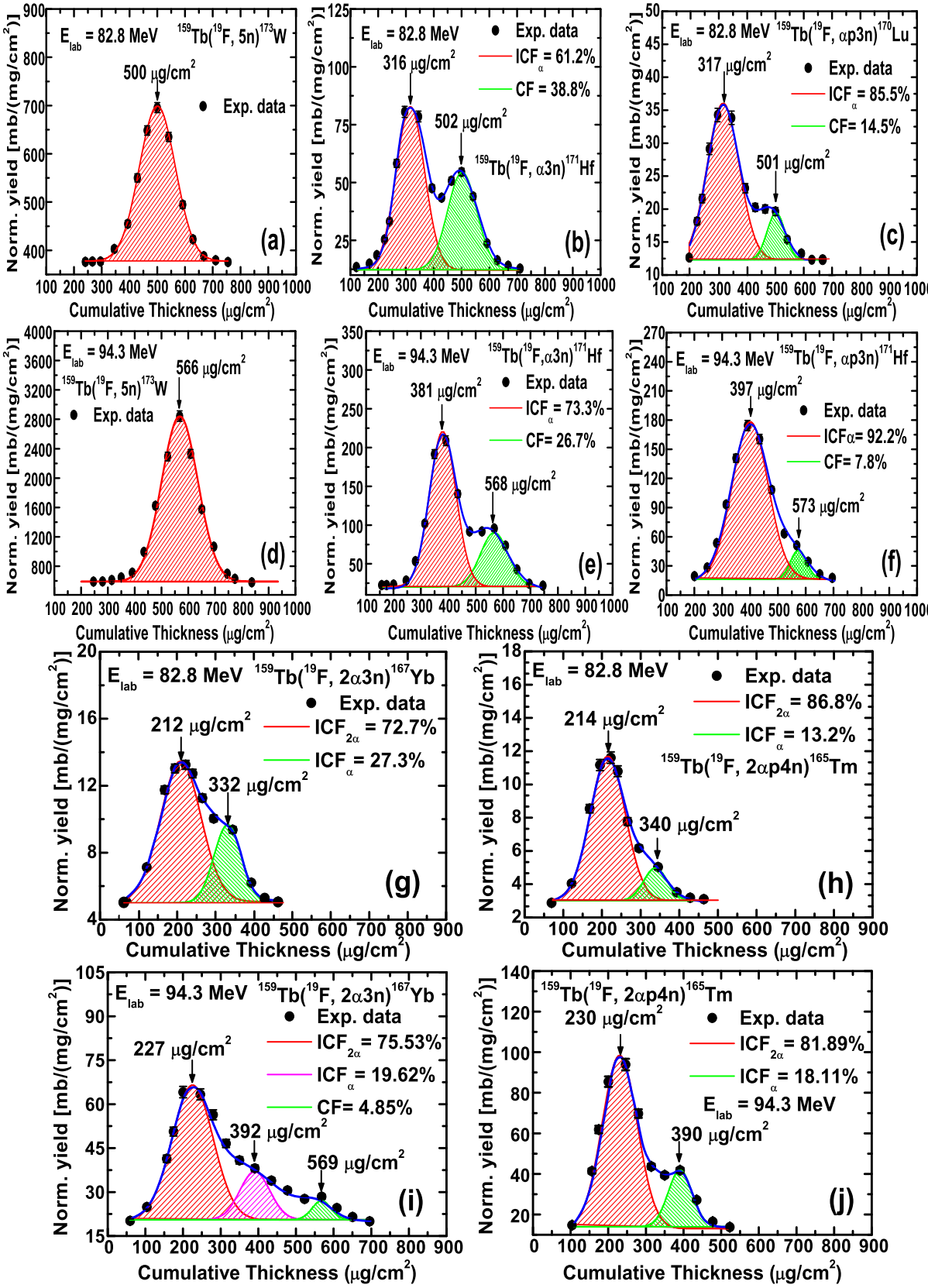

FIG. 4. The experimentally measured FRRD for various residues populated via CF and/or ICF processes at 82.8 MeV and 94.3 MeV beam energy. The size of the circles includes uncertainty in the normalized yield values.

TABLE III. Experimentally measured most probable ranges $R_{p(\text{exp})}$ deduced from FRRD curve and theoretically estimated mean ranges $R_{p(\text{theo})}$ in Al in units of μg/cm^2 for CF and ICF components in the interaction of $^{19}\text{F} + {}^{159}\text{Tb}$.

	$E_{\text{lab}} = 94.3$ MeV			$E_{\text{lab}} = 82.8$ MeV		
Residues	$R^{\text{CF}}_{p(\text{exp})}(R_{p(\text{theo})})$	$R^{\text{ICF}_\alpha}_{p(\text{exp})}(R_{p(\text{theo})})$	$R^{\text{ICF}_{2\alpha}}_{p(\text{exp})}(R_{p(\text{theo})})$	$R^{\text{CF}}_{p(\text{exp})}(R_{p(\text{theo})})$	$R^{\text{ICF}_\alpha}_{p(\text{exp})}(R_{p(\text{theo})})$	$R^{\text{ICF}_{2\alpha}}_{p(\text{exp})}(R_{p(\text{theo})})$
^{174}W($4n$)	567 ± 16 (580)	–	–	500 ± 16(510)	–	–
^{173}W($5n$)	566 ± 17 (580)	–	–	500 ± 17(510)	–	–
^{173}Ta($p4n$)	567 ± 18 (580)	–	–	500 ± 17(510)	–	–
^{171}Hf($\alpha 3n$)	568 ± 17 (580)	381 ± 14(394)	–	502 ± 17(510)	316 ± 17(333)	–
^{170}Hf($\alpha 4n$)	577 ± 17 (580)	398 ± 17(394)	–	500 ± 14(510)	317 ± 17(333)	–
^{170}Lu($\alpha p3n$)	573 ± 12 (580)	397 ± 19(394)	–	500 ± 11(510)	317 ± 17(333)	–
^{167}Yb($2\alpha 3n$)	569 ± 17 (580)	392 ± 15(394)	227 ± 10(227)	–	332 ± 14(333)	212 ± 16(200)
^{167}Tm($2\alpha p2n$)	–	382 ± 15(394)	233 ± 14(227)	–	327 ± 11(333)	199 ± 14(200)
^{165}Tm($2\alpha p4n$)	–	390 ± 15(394)	230 ± 11(227)	–	340 ± 12(333)	214 ± 15(200)

were resolved into two Gaussian peaks by using the ORIGIN software. As a representative case, the measured FRRDs for the residues ^{171}Hf($\alpha 3n$) is shown in Figs. 4(b) and 4(e) at energies 82.8 MeV and 94.3 MeV, respectively. As can be seen from this figure, the FRRDs may be fitted with two Gaussian peaks, one peaking at 502 ± 15 μg/cm^2 and the other at 568 ± 19 μg/cm^2 cumulative thickness for the two beam energies, indicating the full linear momentum transfer events. However, another Gaussian peak at lower cumulative depth of 316 ± 17 and 381 ± 17 μg/cm^2 is also obtained, which corresponds to fusion of ^{15}N (if ^{19}F is assumed to break into $^{14}\text{N} + \alpha$ and ^{15}N fuses) with the target nucleus. The details regarding the α clustering of ^{19}F is well explained by La Cognata *et al.* [20], Buck and Pilt [21], and Goldberg *et al.* [22]. The Gaussian peak at lower cumulative depth shows the partial LMT from projectile to the target nucleus. It is also mentioned that the complete as well as incomplete momentum transfer peaks are centered at the expected position calculated by the SRIM code. As such, these residues may have contributions not only from CF but also from ICF processes. Similar observations for the residues ^{170}Lu populated via $\alpha p3n$ channel has been obtained and is shown in the Figs. 4(c) and 4(f).

Moreover, in order to check the sensitivity of FRRD method, the comparison of experimentally obtained recoil range distributions of the reaction residues have been performed at 82.8 and 94.3 MeV beam energy. In order to verify the observed ranges (R_p^{exp}) of the recoiling residues, the calculations performed (R_p^{theo}) using the code SRIM [23] are compared with observed ranges. These values are given in Table III. The uncertainties in the experimentally measured most probable mean range ($\overline{R}$) has been evaluated [24] using the expression;

$$\overline{R} = \frac{\sigma}{\sqrt{n}}. \tag{3}$$

This is referred to as the standard error of the mean indicated in parenthesis next to the numerical values in Table III. It may also be noted that the error depends on the sample number as one would expect. Further, as n increases, the estimated $\overline{R}$ becomes more precise [24]. As the measurement of FRRD is based on energy/momentum transfer to recoiling residues, hence, the residues traversing with higher energy/momentum may have smaller width. It is due to the fact that the straggling of these residues in the stopping medium is likely to be less as compared to that of residues traveling with lower energy. The observed width for the production of residues ^{173}W($5n$) is found to be larger at lower energy [as shown in Fig. 4(a) at 82.8 MeV] as compared to that of relatively higher energy [as shown in Fig. 4(d) at 94.3 MeV]. The most probable recoil ranges (R_p^{theo}) have been calculated assuming that in case of CF, the incoming projectile completely fuses with the target nucleus and transfers its total linear momentum. Further, an attempt has also been made to check the consistency in the FWHM of the observed FRRDs and the observed FWHM has been found to be consistent for the CF and ICF residues individually. In light of the above discussion, it is clear that the residue ^{173}W populated via $5n$ channel is associated with the full LMT from projectile to target nucleus and may be represented as, $^{19}\text{F} + {}^{159}\text{Tb} \Rightarrow {}^{178}\text{W}^* \Rightarrow {}^{173}\text{W} + 5n$.

Following the above, the FRRDs for the residues viz., ^{174}W($4n$) and ^{173}Ta($p4n$) are found to have a single peak which corresponds to the complete linear momentum transfer from projectile to target nucleus, indicating the production of these residues via CF process only.

The residues ^{171}Hf($\alpha 3n$) may be populated via two different deexcitation processes as;

(i) Fusion of ^{19}F with ^{159}Tb

$$\begin{aligned} {}^{19}\text{F} + {}^{159}\text{Tb} &\Rightarrow {}^{178}\text{W}^* \\ &\Rightarrow {}^{171}\text{Hf} + \alpha 3n \end{aligned}$$

or

(ii) Fusion of ^{15}N with ^{159}Tb with α as spectator

$$\begin{aligned} {}^{19}\text{F}({}^{15}\text{N} + \alpha) &\Rightarrow {}^{15}\text{N} + {}^{159}\text{Tb} \\ &\Rightarrow {}^{174}\text{Hf}^* + \alpha \text{ (as spectator)} \\ &\Rightarrow {}^{171}\text{Hf} + 3n. \end{aligned}$$

Similarly, the FRRDs for other αxn channels have been obtained and resolved into two Gaussian peaks indicating the presence of more than one linear momentum transfer component.

Further, in case of $2\alpha xn$ or $2\alpha pxn$ channels, the measured FRRDs were found to be resolved into three Gaussian peaks. The measured FRRD for residue ^{167}Yb populated via $2\alpha 3n$ is shown in Figs. 4(g) and 4(i) at 82.8 and 94.3 MeV,

respectively. In Fig. 4(g), the peak at cumulative depth 332 ± 14 μg/cm^2 corresponds to partial linear momentum transfer, i.e., fusion of ^{15}N. Another peak at a lower cumulative depth 212 ± 16 μg/cm^2 corresponds to the fusion of ^{11}B with the target nucleus. It may also be stated that the peak at 332 ± 14 μg/cm^2 thickness corresponds to the emission of one α particle from the projectile and the peak at lower thickness 212 ± 16 μg/cm^2 corresponds to the emission of two α particles from the projectile nucleus. It should also be noted that there is no third Gaussian peak at higher cumulative thickness [see Fig. 4(g)], which clearly indicates that the residues ^{167}Yb populated via $2\alpha 3n$ is formed only through the ICF process and there is no or negligible contribution from CF process in the formation of this residue at 82.8 MeV beam energy. However, at higher beam energy of 94.3 MeV, the measured FRRD for the same ^{167}Yb residues is found to be resolved into three Gaussian peaks as shown in Fig. 4(i). In this figure, the peak at 569 ± 12 μg/cm^2 depth corresponds to the full linear momentum transfer (i.e., fusion of ^{19}F with the target nucleus), however, the peak at 392 ± 12 μg/cm^2 depth corresponds to the fusion of ^{15}N and the peak at 227 ± 15 μg/cm^2 depth corresponds to the fusion of ^{11}B with the target nucleus. It should also be inferred from the Fig. 4(i) that at this energy (94.3 MeV), there is contribution from both the CF and ICF processes. Further, the measured FRRDs for residues ^{165}Tm populated via $2\alpha p4n$ channel are also shown in Figs. 4(h) and 4(j) at 82.8 and 94.3 MeV, respectively. It can be clearly seen from this figure that there is no third Gaussian peak at the expected cumulative depth, which indicates that there is no contribution from the CF reactions at these two energies. Hence, the residues ^{165}Tm are populated only via ICF process. The formation of the residues ^{167}Yb populated via $2\alpha 3n$ channel may be explained in three ways as represented below;

(i) Fusion of ^{19}F with ^{159}Tb

$$^{19}\mathrm{F} + {}^{159}\mathrm{Tb} \Rightarrow {}^{178}\overset{*}{\mathrm{W}} \Rightarrow {}^{167}\mathrm{Yb} + 2\alpha 3n$$

or

(ii) Fusion of ^{15}N with ^{159}Tb with α as spectator

$$\begin{aligned} {}^{19}\mathrm{F}({}^{15}\mathrm{N} + \alpha) &\Rightarrow {}^{15}\mathrm{N} + {}^{159}\mathrm{Tb} \\ &\Rightarrow {}^{174}\mathrm{Hf}^* + \alpha \text{ (as spectator)} \\ &\Rightarrow {}^{174}\mathrm{Hf}^* \\ &\Rightarrow {}^{167}\mathrm{Yb} + \alpha 3n \end{aligned}$$

or

(iii) Fusion of ^{11}B with ^{159}Tb with 2α as spectator

$$\begin{aligned} {}^{19}\mathrm{F}({}^{11}\mathrm{B} + 2\alpha) &\Rightarrow {}^{11}\mathrm{B} + {}^{159}\mathrm{Tb} \\ &\Rightarrow {}^{170}\mathrm{Yb}^* + 2\alpha \text{ (as spectator)} \\ &\Rightarrow {}^{167}\mathrm{Yb} + 2\alpha 3n. \end{aligned}$$

The production of same residues via two different channels is analyzed on the basis of break-up fusion model, where it is assumed that the incident projectile ^{19}F breaks up into different fragments when it enters the target nuclear field. The fragments of ^{19}F beam(^{15}N, α) so produced are found to move nearly with the same velocity as that of incoming beam. One of the fragments fuses with the target nucleus forming an incompletely fused composite system, which recoils in the forward direction to conserve linear momentum. It is of primary interest to find out the reactions wise contributions of CF and ICF processes.

In order to deduce the relative contributions of complete and incomplete fusion in various reactions, the experimentally measured FRRDs have been fitted with Gaussian peaks using the software ORIGIN. The graphic software ORIGIN requires the observed intensity distribution of the FRRDs and number of peaks to be fitted, as input data. The software then generates the Gaussian peaks with suitable FWHM to fit the data. The relative contributions of the CF and ICF processes are obtained by dividing the area of the corresponding peak by the total area. The Gaussian curves of various evaporation residues obtained from FRRD are given by;

$$Y = Y_o + \frac{A}{\omega_A^2\sqrt{2\pi}} e^{-(R-R_P)^2/2\pi\omega_A^2}, \tag{4}$$

where R_P is the most probable mean range, ω_A is the width parameter (FWHM) of the distribution and A is the area under the peak. The normalized yield Y may be estimated by the χ square fit (χ^2) of the experimentally determined range distribution and may be given as

$$\chi^2 = \frac{1}{m-p-1}[Y(A) - Y_o(A)]^2. \tag{5}$$

The value of χ^2 was minimized in the analysis using the nonlinear least-square fit routine, keeping the width parameter(ω_A) and most probable mean range (R_P) as a free parameter. As already mentioned before, the residues involving α-emitting channels show more than one FRRD components. In such cases, the experimentally measured FRRDs have been fitted using the multipeak option in a similar way as mentioned above. The contributions from different fusion components (CF, ICF$_\alpha$, and ICF$_{2\alpha}$) have been obtained by dividing the area under the peak for the fused component with the total area of associated with experimental data. Further, the range integrated cross sections for different residues have been obtained and compared with the theoretical predictions of the code PACE4 [16] as shown in Table IV. It has been observed from this table that the contribution from CF (from xn and pxn channels) component satisfactorily matches with the theoretical predictions of PACE4. However, the contribution of ICF reactions could not be reproduced by the theoretical model code because it does not take into account the contributions from ICF reactions. It may, however, be remarked that the ICF contribution deduced as indicated above and given in Table IV are based on the direct measurements of the contribution due to CF and ICF residues.

B. Consistency in the present measurements

The excitation functions (EFs) of various reaction residues viz., ^{174}W($4n$), ^{173}W($5n$), ^{172}W($6n$), ^{173}Ta($p4n$), ^{171}Hf($\alpha 3n$), ^{170}Hf($\alpha 4n$), ^{170}Lu($\alpha p3n$), ^{167}Yb($2\alpha 3n$), ^{167}Tm($2\alpha p2n$), and ^{165}Tm($2\alpha p4n$) populated via CF and/or ICF modes in $^{19}\mathrm{F} + {}^{159}\mathrm{Tb}$ system were measured in the energy range

TABLE IV. Experimentally measured forward recoil range integrated cross section ($\sigma_{\rm exp}^{\rm FRRD}$) and theoretically calculated cross section ($\sigma_{\rm theo}^{\rm PACE}$) in units of *mb* at 82.8 and 94.3 MeV beam energy.

Residues	$E_{\rm lab}$ = 82.8 MeV		$E_{\rm lab}$ = 94.3 MeV	
	$\sigma_{\rm exp}^{\rm FRRD}$	$\sigma_{\rm theo}^{\rm PACE}$	$\sigma_{\rm exp}^{\rm FRRD}$	$\sigma_{\rm theo}^{\rm PACE}$
^{174}W($4n$)	133 ± 9	125	68.3 ± 5	73
^{173}W($5n$)	52 ± 4	50	382.3 ± 27	407
^{174}Ta^{cum}($p4n$)	105 ± 7	–	407.7 ± 29	–
^{174}Ta^{ind}($p4n$)	7.86 ± 0.6	7.5	10.4 ± 0.7	10
^{171}Hf($\alpha 3n$)	13 ± 1	6	33.5 ± 2.4	17
^{170}Hf($\alpha 4n$)	1.8 ± 0.1	0.1	78 ± 5	11
^{170}Lu($\alpha p3n$)	1.02 ± 0.1	–	25 ± 2	1
^{167}Yb($2\alpha 3n$)	1.4 ± 0.01	–	7.5 ± 0.5	0.4
^{167}Tm($2\alpha p2n$)	9 ± 0.6	–	18 ± 1	–
^{165}Tm($2\alpha p2n$)	1.13 ± 0.1	–	12.2 ± 1	–

≈81–110 MeV [5]. The experimental EFs of residues populated via xn/pxn channels were found to be well reproduced by the predictions of code PACE4, confirming the production of these residues solely via complete fusion process. However, the observed enhancement in the EFs of α-emitting channels as compared to PACE4 predictions has been attributed to incomplete fusion process.

In the present work, an attempt has been made to have a better insight on the ICF values obtained from the analysis of FRRD data. The incomplete fusion strength function $F_{\rm ICF}$, a measure of strength of ICF relative to the total fusion is deduced using the expression $F_{\rm ICF}$=$\sum \sigma_{\rm ICF}^{\rm exp}/\sigma_{TF}$. Here, $\sigma_{\rm ICF}^{\rm exp}$ is the deduced experimental value of ICF cross section and σ_{TF} ($= \sum \sigma_{\rm CF}^{\rm exp} + \sum \sigma_{\rm ICF}^{\rm exp}$) is the total fusion cross section. The $F_{\rm ICF}$ obtained with the help of two different measurements *viz.* (i) measurement of EFs and (ii) from the present measurement of FRRDs are compared and plotted as a function of center of mass energy ($E_{C.M.}$) and $v_{\rm rel}$ as shown in Fig. 5. In this figure, the red vertical bars are obtained from the experimentally measured EF data, however, on the other hand, the percentage relative contribution of ICF ($F_{\rm ICF}$) in case of FRRD measurement is shown by blue color vertical bars. Also, the channels that could not be observed, their cross section values were taken from the code PACE4 to estimate ICF strength function in both the cases. Moreover, as can be seen from Fig. 5, the $F_{\rm ICF}$ increases as the beam energy (or $v_{\rm rel}$) is increased suggesting its dependence on projectile energy. Further, it may also be pertinent to mention that both the measurements of FRRDs and EFs gives nearly the same value of $F_{\rm ICF}$ at the studied energies within the experimental uncertainty, strengthening thereby the present measurements and self-consistency of the data. Further, it may also be remarked that Morgenstern *et al.*, [25] in their pioneer work showed that ICF fraction increases at $v_{\rm rel} \geqslant 0.06$c, however, in the present work a significant contribution from ICF processes even below $v_{\rm rel} = 0.06$c has been observed.

In order to explore the effects of projectile breakup on fusion cross section, an attempt has also been made to deduce the suppression of complete fusion cross section data from the measurement of FRRD also for the presently studied

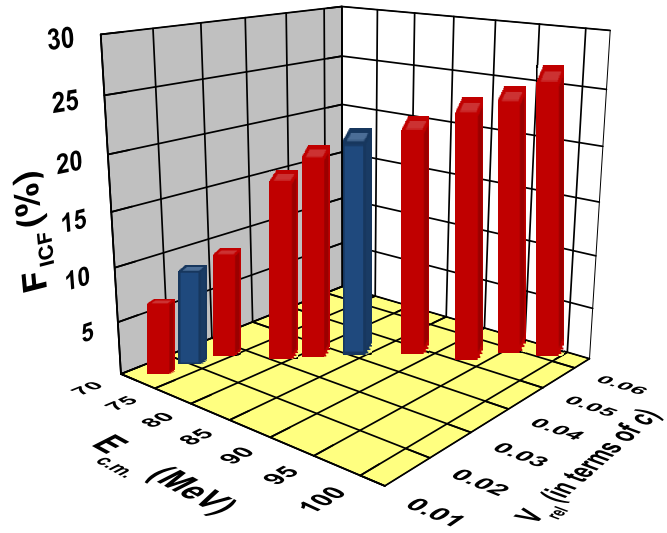

FIG. 5. A comparison of incomplete fusion strength function ($F_{\rm ICF}$) deduced from the analysis of EF and FRRD measurement (for more details, see text).

^{19}F + ^{159}Tb system. In view of the above, the total fusion cross section data ($\sum \sigma_{\rm CF}$) has been obtained and compared with the theoretical predictions of code CCFULL [26] as shown in Fig. 6. The circular shaped red data points shown in this figure are obtained by summing all the CF channels obtained from the measurement of EFs [5] whereas square shaped blue data points are obtained from the FRRD measurement done in the present work.

As can be seen from Fig. 6 that the experimental fusion cross section data for EF and also for FRRD data are in good agreement with the predictions of the code CCFULL over the entire range of energy, justifying the validity of the present measurements. In the coupled-channels (CC) formalism, the Wood-Saxon (WS) potential, which is a deep attractive potential, is used as a real nuclear potential and its depth (V_o) is chosen to reproduce the experimental cross section. The other two parameters used in CCFULL code are radius parameter

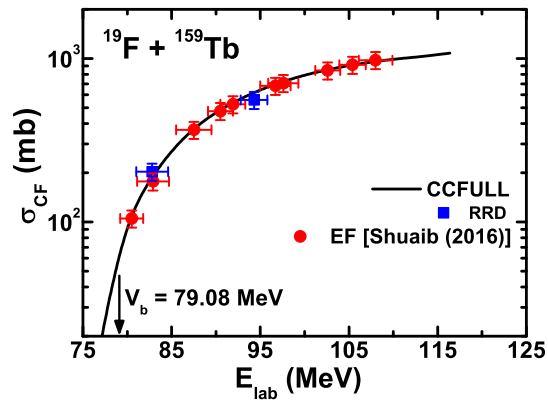

FIG. 6. The experimentally measured total complete fusion cross section ($\sum \sigma_{\rm CF}$) (blue data points) plotted as a function of incident beam energy. The red data points represent the data obtained from EF measurements [5] (for more details, see text).

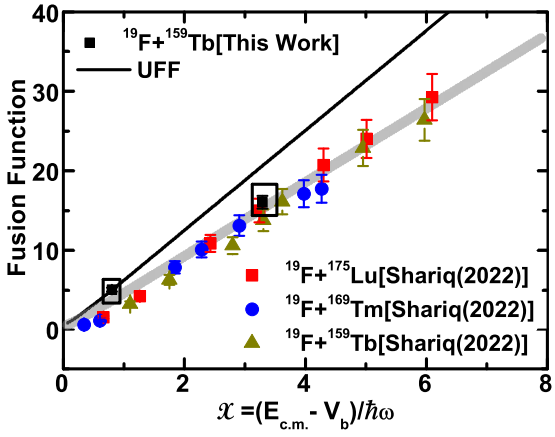

FIG. 7. The experimental fusion function data obtained from range integrated cross section and compared with the EF data of other systems [30]. The black solid line denotes the UFF given in Ref. [27].

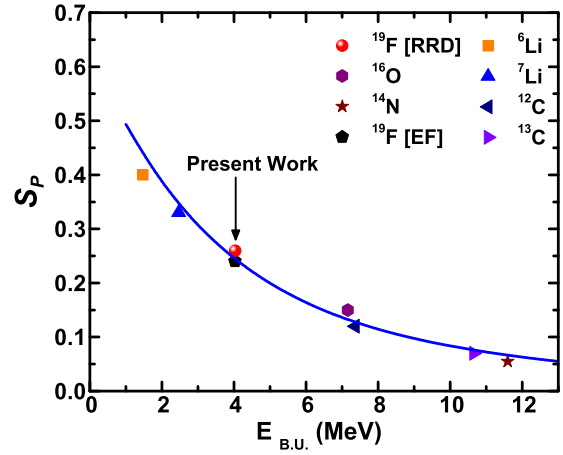

FIG. 8. The deduced suppression obtained for the present work using FRRD measurement and compared with the data of other systems obtained from EF measurement. The blue solid line represents the empirical relation given in Ref. [30].

(r_o) and diffuseness parameter (a_o). The diffuseness parameter affects the slope of the nuclear potential in the surface region, and thus the curvature of the effective potential. In order to calculate fusion cross section, the values of various parameters V_o, r_o, and a_o used in CCFULL code are taken to be 64.8 MeV, 1.178 fm, and 0.659 fm respectively. The coupled channels calculations are found to explain the fusion cross section data, in general, at above-barrier energies reasonably well. Further, in order to obtain the suppression of fusion data, it is necessary to eliminate the different geometrical and static effects arising due to the potential acting between the two nuclei. Hence, method suggested by Canto *et al.*, [27–29] has been adopted in the present work.

The experimental fusion function has been deduced from range integrated cross section data of FRRD for $^{19}\mathrm{F}+^{159}\mathrm{Tb}$ system and plotted as a function of dimensionless variable x (excess center-of-mass energy above Coulomb barrier normalized to barrier curvature) [27] as shown in Fig. 7. The experimental fusion function of the present system along with $^{19}\mathrm{F}+^{169}\mathrm{Tm}$, $^{19}\mathrm{F}+^{175}\mathrm{Lu}$ systems studied earlier [30] is also shown in this figure. The black solid line in this figure denotes the universal fusion function (UFF) [27]. The black squares enclosed in black rectangular box are obtained from present FRRD measurements. As can be seen from this figure that there is a significant suppression in experimental fusion function data deduced from FRRD with respect to UFF particularly at higher energy. This suppression may be attributed to the loss of flux due to ICF processes becoming dominant at relatively higher energies. As a result, a component of cross section due to incomplete fusion of projectile may reduce the experimental fusion cross section data. The suppression obtained in the present work is in good agreement with the available similar data [30]. Further, in Fig. 7 the shaded area represents the suppression of cross section data obtained by multiplying the UFF by 0.74 and 0.76.

Further, an attempt has also been made to correlate the suppression obtained from fusion function analysis for the present measurement with the break-up threshold energy of the projectile [31]. The deduced suppression factors has been plotted as a function of break-up threshold energy of different projectiles and is shown by blue color solid line in Fig. 8. This exponential plot indicates that if the break-up threshold energy of a projectile is larger, suppression is lower. It may be because of the fact that, when break-up threshold energy is higher, more energy would be required in order to separate out an α particle from the projectile leading to the lower value of suppression. Further, it should also be noted that there is a one-to-one correspondence between suppression (S_P) and the probability of ICF (P_{ICF}). Larger suppression indicates that the probability of ICF would be more and vice versa. This clearly justifies the self-consistency and reliability of the present analysis done using the FRRD measurement.

IV. CONCLUSIONS

In the present work, the forward recoil range distribution of nine reaction residues viz., ^{174}W($4n$), ^{173}W($5n$), ^{173}Ta($p4n$), ^{171}Hf($\alpha 3n$), ^{170}Hf($\alpha 4n$), ^{170}Lu($\alpha p3n$), ^{167}Yb($2\alpha 3n$), ^{167}Tm($2\alpha p2n$), and ^{165}Tm($2\alpha p4n$) populated in the interaction of ^{19}F with ^{159}Tb target have been measured at energies ≈83 and 94 MeV. A significant contribution from ICF reactions is found to play an important role in the production of different residues. It has strongly been revealed that there is a transfer of partial momentum along with full momentum from projectile to target in case of α-emitting channels associated with ICF reactions. The different partial LMT components corresponds to the break up and fusion of ^{19}F into ^{15}N and ^{11}B with the target nucleus. Further, the relative contribution of complete and/or incomplete fusion components have also been obtained. Moreover, an attempt has also been made to obtain the suppression of fusion cross section data using the FRRD measurements and it has been observed that there is a suppression of about ≈24% in fusion cross data as compared to the benchmark curve universal fusion function (UFF). This suppression may be attributed to the contributions from the incomplete fusion reactions. Moreover, it may also be concluded that, as the

break-up threshold energy of the projectile decreases, the fusion may get more suppressed giving way to enhancement in the break-up probability. The variation of suppression in fusion cross section data as function of break-up threshold of the projectile has been observed to follow an exponential relation. From the analysis of data it may be concluded that the break up of projectile may take place as it comes in the vicinity of target nucleus. It may be due to the fact that as the projectile approaches the target nucleus, the Coulomb repulsion acting between them increases and may give rise to the prompt break up of projectile into fragment(s) and one of the fragment(s) fuses with the target nucleus leading to ICF processes. The critical angular momentum $\ell_{\rm crit}$ for the present system at which the pocket in the entrance-channel potential nearly vanishes has been calculated using the prescription of Wilzyanski *et al.* [7] and is found to be 79 $\hbar$. The values of $\ell_{\rm max}$ at two respective energies (82.8 and 94.3 MeV) in the present work are $\approx$22 $\hbar$ and 40 $\hbar$, respectively, which are less than the $\ell_{\rm crit}$ (79 $\hbar$) for fusion to occur in the present system. The observation of ICF for energies where $\ell_{\rm max} < \ell_{\rm crit}$ suggests that a significant number of ℓ-waves below $\ell_{\rm crit}$ may contribute to ICF reactions.

In order to achieve a better understanding and more conclusive picture of ICF reaction dynamics, more experimental data covering a broader range of nuclei is required. Further, complimentary experiments such as particle-γ coincidence for both loosely as well as strongly bound projectiles may give a detailed insight of the ICF reaction dynamics. The new experimental data may help in the refinement of existing theoretical models and in developing systematics at energies $\approx$4–7 MeV/nucleon.

ACKNOWLEDGMENTS

The authors thank the Director, IUAC, New Delhi, India and the Chairperson, Department of Physics, Aligarh Muslim University, Aligarh (U.P), India for providing all the necessary facilities to carry out this work. M.S.A. and B.P.S. thank the DST-SERB for providing financial support under the Project No. CRG/2020/000136.

[1] E. Holub, D. Hilscher, G. Ingold, U. Jahnke, H. Orf, and H. Rossner, Phys. Rev. C **28**, 252 (1983).
[2] M. Cavinato, E. Fabrici, E. Gadioli, E. Gadioli Erba, P. Vergani, M. Crippa, G. Colombo, I. Redaelli, and M. Ripamonti, Phys. Rev. C **52**, 2577 (1995).
[3] P. Vergani, E. Gadioli, E. Vaciago, E. Fabrici, E. Gadioli Erba, M. Galmarini, G. Ciavola, and C. Marchetta, Phys. Rev. C **48**, 1815 (1993).
[4] D. J. Parker, J. J. Hogan, and J. Asher, Phys. Rev. C **35**, 161 (1987).
[5] Mohd. Shuaib, V. R. Sharma, A. Yadav, P. P. Singh, M. K. Sharma, D. P. Singh, R. Kumar, R. P. Singh, S. Muralithar, B. P. Singh, and R. Prasad, Phys. Rev. C **94**, 014613 (2016).
[6] T. Inamura, M. Ishihara, T. Fukuda, T. Shimoda, and H. Hiruta, Phys. Lett. B **68**, 51 (1977).
[7] J. Wilczyński, K. Siwek-Wilczyńska, J. van Driel, S. Gonggrijp, D. C. J. M. Hageman, R. V. F. Janssens, J. Łukasiak, and R. H. Siemssen, Phys. Rev. Lett. **45**, 606 (1980).
[8] I. Tserruya, V. Steiner, Z. Fraenkel, P. Jacobs, D. G. Kovar, W. Henning, M. F. Vineyard, and B. G. Glagola, Phys. Rev. Lett. **60**, 14 (1988).
[9] T. Udagawa and T. Tamura, Phys. Rev. Lett. **45**, 1311 (1980).
[10] J. R. Wu and I. Y. Lee, Phys. Rev. Lett. **45**, 8 (1980).
[11] J. Wilczynski, K. Siwek-Wilczynska, J. Van Driel, S. Gonggrijp, D. C. J. M. Hageman, R. V. F. Janssens, J. Łukasiak, R. H. Siemssen, and S. Y. Van Der Werf, Nucl. Phys. A **373**, 109 (1982).
[12] K. Siwek-Wilczynska, E. H. du Marchie van Voorthuysen, J. van Popta, R. H. Siemssen, and J. Wilczyski, Phys. Rev. Lett. **42**, 1599 (1979).
[13] M. Blann, Phys. Rev. C **23**, 205 (1981).
[14] T. Otsuka and Kichinosuke Harada, Phys. Lett. B **121**, 106 (1983).
[15] B. P. Singh, M. K. Sharma, and R. Prasad, *Pre-Equilibrium Emission in Nuclear Reactions: Fundamentals, Measurements and Analysis* (IOP Publishing, 2022).
[16] A. Gavron, Phys. Rev. C **21**, 230 (1980).
[17] N. G. Puttaswamy, N. M. Badiger, M. Raja Rao, D. K. Avasthi, A. Tripathi, D. Kabiraj, and S. Venkataramanan, in *DAE Symposium on Nuclear Physics, Bombay, 1991*, Vol. 34B (DAE, Mumbai, 1991).
[18] E. T. Subramaniam, K. Rani, B. P. Ajith Kumar, and R. K. Bhowmik, Rev. Sci. Instrum. **77**, 096102 (2006).
[19] U. Gupta, P. P. Singh, D. P. Singh, M. K. Sharma, A. Yadav, R. Kumar, B. P. Singh, and R. Prasad, Nucl. Phys. A **811**, 77 (2008).
[20] M. La Cognata *et al.*, Phys. Rev. C **99**, 034301 (2019).
[21] B. Buck and A. A. Pilt, Nucl. Phys. A **280**, 133 (1977).
[22] V. Z. Goldberg, A. K. Nurmukhanbetova, A. Volya, D. K. Nauruzbayev, G. E. Serikbayeva, and G. V. Rogachev, Phys. Rev. C **105**, 014615 (2022).
[23] SRIM code, The Stopping and Range of Ions in Matter code: http://www.srim.org/SRIM/SRIMLEGL.htm.
[24] W. R. Leo, *Techniques for Nuclear and Particle Physics Experiments* (Springer, Berlin, 2010).
[25] H. Morgenstern, W. Bohne, W. Galster, K. Grabisch, and A. Kyanowski, Phys. Rev. Lett. **52**, 1104 (1984).
[26] K. Hagino, N. Rowley, and A. T. Kruppa, Comput. Phys. Commun. **123**, 143 (1999).
[27] L. F. Canto, P. R. S. Gomes, J. Lubian, L. C. Chamon, and E. Crema, Nucl. Phys. A **821**, 51 (2009), and references therein.
[28] L. F. Canto, P. R. S. Gomes, J Lubian, L. C. Chamon, and E Crema, J. Phys. G: Nucl. Part. Phys. **36**, 015109 (2009).
[29] C. Y. Wong, Phys. Rev. Lett. **31**, 766 (1973).
[30] M. S. Asnain, Mohd. Shuaib, I. Majeed, M. K. Sharma, V. R. Sharma, A. Yadav, D. P. Singh, P. P. Singh, S. Kumar, R. Kumar, B. P. Singh, and R. Prasad, Phys. Rev. C **105**, 014609 (2022).
[31] B. Wang, W. J. Zhao, P. R. S. Gomes, E. G. Zhao, and S. G. Zhou, Phys. Rev. C **90**, 034612 (2014).